water

MDPI

Article

Polyethyleneimine-Modified Magnetic Multivalent Iron Derived from Iron-Based Waterwork Sludge for Cr(VI) Adsorption and Reduction

Jingxi Tie [1], Huawen Wang [1], Junkai Zheng [2], Mengjia Yan [1], Sihao Shao [1], Xiaohan Duan [3] and Zhaoyong Ye [1,*]

[1] School of Environmental and Municipal Engineering, North China University of Water Resources and Electric Power, Zhengzhou 450046, China; tjx@ncwu.edu.cn (J.T.); wanghuawen2025@163.com (H.W.); 18790217066@163.com (M.Y.); 15039053275@163.com (S.S.)
[2] College of Water Conservancy and Hydropower Engineering, Hohai University, Nanjing 210024, China; zhengjunkai9500@gmail.com
[3] School of Environment and Ecology, Henan Vocational College of Water Conservancy and Environment, Zhengzhou 450008, China; b2019081505@stu.ncwu.edu.cn
* Correspondence: yezhaoyong123@126.com

Abstract

In this study, activated carbon, iron-based waterwork sludge, and polyethyleneimine (PEI) were employed as the primary raw materials to synthesize the composite PEI@MMI(800) under the optimized conditions identified through experimental investigations. The resulting composite was employed as an adsorbent for static Cr(VI) adsorption tests. The results demonstrated that increasing the pH from 2 to 9 significantly decreased the Cr(VI) adsorption capacity from 41.09 mg/g to 15.75 mg/g. The adsorption process was well described by both the pseudo-second-order kinetic model and the Langmuir isotherm model. Thermodynamic analysis revealed that the adsorption process was spontaneous and endothermic in nature. The presence of anions (Cl^-, SO_4^{2-}, and PO_4^{3-}) negatively impacted Cr(VI) adsorption, with their inhibitory effects following the order $Cl^- < SO_4^{2-} < PO_4^{3-}$. Moreover, higher concentrations of these anions led to reduced Cr(VI) adsorption efficiency. After six cycles of use, PEI@MMI(800) retained 79.80% of its initial Cr(VI) adsorption capacity, indicating a loss of 20.20%. Based on the comprehensive characterization of the adsorbent and the results of the Cr(VI) adsorption tests, it was concluded that the removal of Cr(VI) by PEI@MMI(800) involved a combination of electrostatic adsorption, chelation of Cr(VI) by PEI, and reduction of Cr(VI) to Cr(III).

Keywords: polyethyleneimine; magnetic multivalent iron; iron-based waterwork sludge; Cr(VI); adsorption; reduction

check for updates

Academic Editor: Alessandro Erto

Received: 4 April 2025
Revised: 26 June 2025
Accepted: 27 June 2025
Published: 29 June 2025

Citation: Tie, J.; Wang, H.; Zheng, J.; Yan, M.; Shao, S.; Duan, X.; Ye, Z. Polyethyleneimine-Modified Magnetic Multivalent Iron Derived from Iron-Based Waterwork Sludge for Cr(VI) Adsorption and Reduction. *Water* **2025**, *17*, 1945. https://doi.org/10.3390/w17131945

Copyright: © 2025 by the authors. Licensee MDPI, Basel, Switzerland. This article is an open access article distributed under the terms and conditions of the Creative Commons Attribution (CC BY) license (https://creativecommons.org/licenses/by/4.0/).

1. Introduction

Aqueous hexavalent chromium (Cr(VI)) has raised global concern owing to its high toxicity and mobility, carcinogenic, mutagenic, and teratogenic effects [1–3]. Consequently, numerous countries have prioritized the regulation of Cr(VI) levels, with the World Health Organization (WHO) setting a maximum acceptable concentration of 0.05 mg/L in water [4]. Aqueous Cr(VI) is released from a wide range of industrial sectors, including mining, leather tanning, wood preservation, electroplating, and textile printing and dyeing, etc. [1,3]. To mitigate its adverse impacts on the environment and living organisms, it is imperative to develop efficient and cost-effective methods for removing Cr(VI) from aqueous solutions.

Several techniques have been developed to remove harmful Cr(VI) from water, such as microbial treatment, adsorption, electrochemical treatment, ion exchange, and membrane filtration [5]. Among these, adsorption stands out as a highly attractive method due to its high efficiency, ease of operation, and low cost [6,7]. However, adsorption merely transfers Cr(VI) from water to a solid adsorbent, concentrating it on the surface while retaining its toxicity.

In comparison to Cr(VI), Cr(III) is not only less active, less mobile, and less toxic, but also an essential trace element involved in the metabolism of protein, fat, and glucose [8,9]. As a result, developing an adsorbent capable of adsorbing and reducing Cr(VI) to Cr(III) is more desirable.

Low-valent Fe, such as Fe^0 and Fe(II), has been shown to effectively remove Cr(VI) by reducing it to Cr(III) [10–12]. However, the conventional production of Fe^0 and Fe(II) typically relies on iron salts such as $FeCl_3$ and $FeSO_4 \cdot 7H_2O$ [9,13], which can lead to chemical consumption and secondary contamination.

Iron-based waterwork sludge (IBWS) is a Fe-rich solid waste generated from a drinking water treatment plant using iron chemicals for water purification. The proper disposal of IBWS is a significant concern due to its large-scale production. Currently, its discharge into water bodies, sewers, or landfills poses potential environmental risks.

Interestingly, IBWS can be converted into Fe_3O_4 in N_2 atmosphere or reduced to Fe^0 in a reductive environment [14,15]. These low-valent iron species can effectively reduce Cr(VI) to Cr(III), offering a promising approach to address both Cr(VI) removal and the sustainable management of IBWS.

Polyethylenimine (PEI) has recently garnered significant attention as a polymer for the development of functional adsorbents, primarily due to its ability to effectively remove pollutants through chelation and electrostatic interactions. These interactions are facilitated by the abundant amine groups present in its structure [16,17]. For instance, Yoo et al. utilized PEI-functionalized carboxymethylcellulose beads to adsorb Hg(II), achieving a predicted maximum adsorption capacity of 313.1 mg/g [16]. Similarly, Xu et al. developed PEI-grafted styrene–maleic anhydride copolymer adsorbents for the removal of reactive black 5 dye, with a remarkable maximum adsorption capacity of 1809.3 mg/g [18].

In this study, IBWS was first reduced by activated carbon (AC) under a nitrogen atmosphere, followed by modification with PEI. The resulting composite was then used as an adsorbent to evaluate its performance in adsorbing and reducing Cr(VI). Additionally, the study investigated several influencing factors, including solution pH, reaction time, Cr(VI) concentration, and the presence of co-existing anions. The mechanisms underlying Cr(VI) removal were also explored.

2. Materials and Methods

2.1. Adsorbent Preparation

IBWS and AC were both sieved through a 60-mesh sieve. The sieved materials were blended at various mass ratios (m_{IBWS}:m_{AC} = 3:1, 3:2, 3:3, 3:4, 3:5, 3:6, 3:7, 3:8, and 3:9). Each mixture was calcined in a N_2 atmosphere in a tube furnace at different temperatures (350 °C, 500 °C, 650 °C, 800 °C, and 950 °C). The temperature was increased at a rate of 15 °C/min and maintained at the target temperature for 180 min. After cooling, the calcined composite was sieved through the same 60-mesh sieve to obtain the magnetic multivalent iron, denoted as MMI.

For the modification of MMI with PEI (molecular weight: 600), 100 mL of PEI solution with various mass fractions (0.5%, 1%, 1.5%, and 2.0%) was added to a three-necked flask containing 1 g of MMI. The mixture was heated to 50 °C and reacted at this temperature for 6 h under vigorous stirring. The pH of the mixture was then adjusted to approximately 8.5

using 1 M HCl solution. Subsequently, 20 mL of glutaraldehyde (GA) solution (50% mass fraction) was added, and the reaction was continued for an additional 8 h. The resulting composite was washed with deionized water several times to remove excess PEI and then dried under vacuum at 70 °C for 12 h to obtain the final adsorbent, denoted as PEI@MMI. The whole process is described in Figure 1.

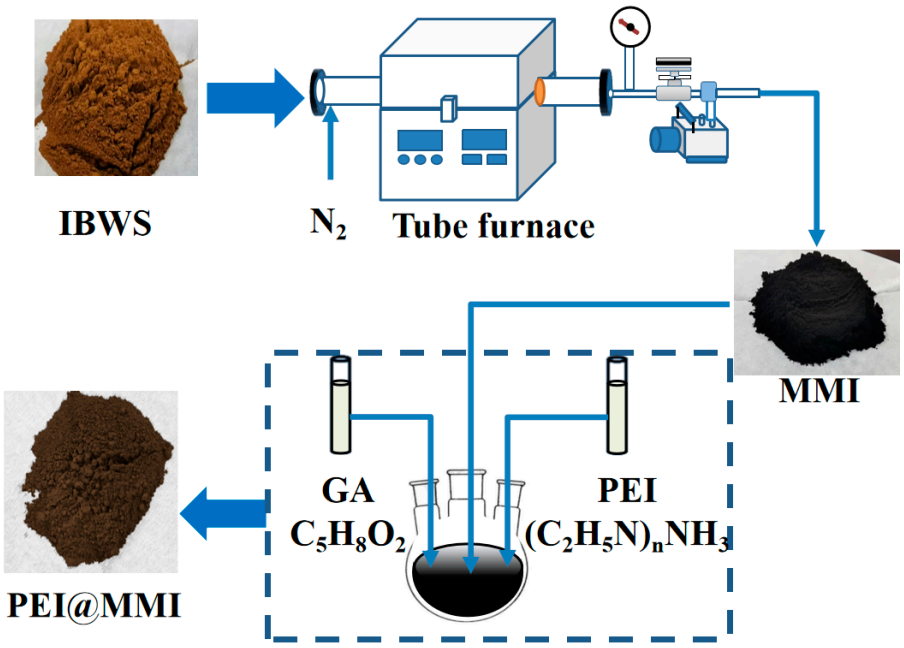

Figure 1. The schematic diagram of adsorbent preparation.

2.2. Preparation of Cr(VI)-Containing Solution

The Cr(VI)-containing solution used in this study was synthesized by dissolving $K_2Cr_2O_7$ (AR, Tianjin Kermel Chemical Reagent Co., Ltd., Tianjin, China) into deionized water, and the pH value of the solution was adjusted using 0.1 mol/L HCl (AR, Guangzhou Chemical Reagent Factory, Guangzhou, China) and NaoH (AR, Tianjin Kermel Chemical Reagent Co., Ltd., Tianjin, China) solutions, yielding the Cr(VI) solution.

2.3. Cr(VI) Adsorption Experiments

A stoppered flask containing 20 mL of an artificial Cr(VI) solution (C_0 = 20 mg/L–100 mg/L) and 0.05 g of the adsorbent was placed in a shaker and agitated at 120 rpm at temperatures of 15 °C, 25 °C, and 35 °C for varying durations. After the reaction, the residual Cr(VI) concentration in the solution was measured after filtering through a 0.45 μm filter. Each experiment was conducted in triplicate, and the average values were used for analysis.

2.4. Adsorbent Characterization

The adsorbents before Cr(VI) adsorption were characterized using X-ray diffraction (XRD, ZSX Primus II, Tokyo, Japan), vibrating sample magnetometry (VSM, Lake Shore 7404, Westerville, OH, USA), zeta potential analysis (Particle Metrix GmbH, Germany), and an automatic specific surface area analyzer (BELSORP-max, MicrotracBEL, Osaka, Japan). The adsorbents before and after Cr(VI) adsorption were characterized using scanning electron microscopy (Zeiss Gemini SEM 500, Bavaria, Germany); the surface elements were analyzed using SEM-EDS (Ultim Max 100, Oxfordshire, British), Fourier-transform infrared spectroscopy (FTIR, Thermo Fisher IS50, Waltham, MA, USA), and X-ray photoelectron spectroscopy (XPS, Thermo Scientific Escalab 250Xi+, Waltham, MA, USA).

2.5. Regeneration and Reuse of the Adsorbent

The adsorbed materials were first separated and immersed in a 0.5 mol/L NaOH solution, where they underwent ultrasonic desorption treatment at 25 °C for 3 h. Following this, the materials were collected, washed thoroughly with deionized water to remove any residual NaOH, and then transferred to 50 mL of an HCl solution with a pH of 4. The adsorbent was reacted in this solution at 25 °C, with continuous stirring at 120 rpm for 3 h. The solid phase was subsequently separated and rinsed with distilled water until the pH of the rinse water stabilized. The adsorbent was then dried in a vacuum oven at 70 °C for 12 h and subsequently sieved through a 60-mesh screen. The resulting materials were used as adsorbents, and adsorption experiments were conducted using the same methods described above.

3. Results and Discussion

3.1. Adsorbent Preparation

Figure 2a presents the Cr(VI) adsorption performance of adsorbents manufactured at temperatures ranging from 350 °C to 950 °C, using raw materials composed of IBWS and AC mixed at mass ratios of IBWS:AC = 3:1, 3:2 and 3:3. As shown in the figure, the Cr(VI) uptake capacity of all MMI samples increased with both the IBWS:AC ratio and the pyrolysis temperature. Given its energy efficiency and superior Cr(VI) removal performance, and the easier magnetic separation of the adsorbent, a pyrolysis temperature of 800 °C was selected for further investigation.

Figure 2b illustrates the influence of the m_{MMI}:m_{AC} on Cr(VI) adsorption by MMIs synthesized at 800 °C. The results indicate that all adsorbents prepared using a combination of IBWS and AC demonstrated significantly enhanced Cr(VI) removal performance compared to IBWS alone, thereby validating the effectiveness of the adsorbent synthesis approach. Notably, the MIBWS sample prepared with a mixing ratio of IBWS:AC = 3:5 achieved the highest Cr(VI) uptake capacity of 21.58 mg/g. Additionally, as the IBWS:AC ratio increased from 3:2 to 3:5, the magnetism of the adsorbents also increased from 18.36 emu/g to 30.68 emu/g (Figure 2c), facilitating more efficient separation of the adsorbent from water. Based on these findings, the optimal mixing ratio for adsorbent preparation was determined to be a mass ratio of IBWS:AC = 3:5.

To enhance the Cr(VI) adsorption capability of MMI, PEI solutions at various concentrations were used for modification. As shown in Figure 2d, PEI modification significantly improved the Cr(VI) adsorption capacity of the composites, increasing it from 21.76 mg/g to 31.57 mg/g. Additionally, the magnetism of the resulting adsorbents also decreased from 17.6 emu/g to 11.0 emu/g as the PEI mass fraction was raised from 0% to 2% (Figure 2e). Considering both the enhanced Cr(VI) adsorption and the maintained magnetism of the composite, a 2% PEI solution was selected for further modification.

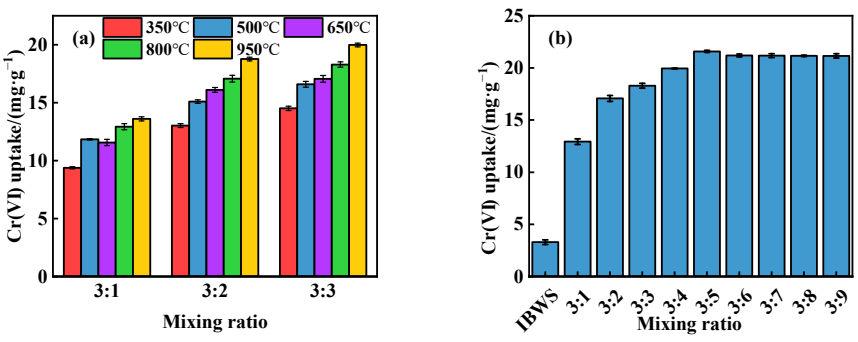

Figure 2. *Cont.*

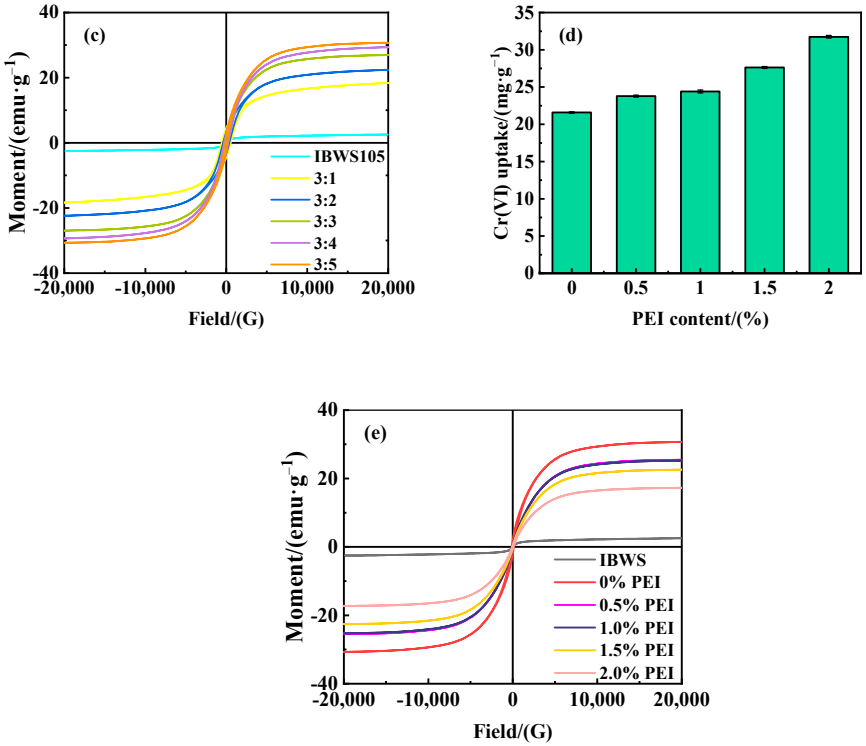

Figure 2. Determination of the optimal condition for adsorbent preparation based on Cr(VI) adsorption: Influence of calcination temperatures on Cr(VI) adsorption (**a**), influence of IBWS:AC on Cr(VI) adsorption (**b**), VSM curves of composite prepared at different m_{IBWS}:m_{AC} (**c**), PEI content on Cr(VI) adsorption (**d**) (pH = 5.1,C_0 = 100 mg/l), and VSM curves of composite prepared using PEI with different contents different mass raito of IBWS:AC (**e**).

3.2. Adsorbent Characterization

As shown in Figure 3, the PEI@MMI(800) sample exhibited a Type IV N_2 adsorption–desorption isotherm and an H_4-type hysteresis loop. Its specific surface area (S_{BET}), total pore volume (V_{tot}), and average pore size were 88.05 m^2/g, 0.12 cm^3/g, and 5.25 nm, respectively. These characteristics indicate that the adsorbent is a typical material with both micropores and mesopores.

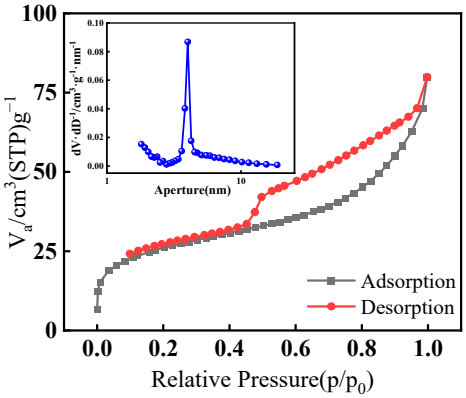

Figure 3. N_2 adsorption–desorption curves of PEI@MMI(800).

3.2.1. SEM

Figure 4a,b present the SEM images of the material prior to adsorption. As depicted, the surface of PEI@MMI(800) was densely populated with small particles that were tightly agglomerated, giving rise to a highly textured and rough surface. Moreover, a multitude of pores of diverse sizes were randomly interspersed among these particles. Following the

completion of the adsorption process, a notable reduction in the number of surface pores was observed. This phenomenon was likely attributed to the adsorption of Cr(VI) onto the composite surface, effectively blocking the pores (Figure 4c,d). As depicted in Figure 4e, the pristine PEI@MMI(800) initially exhibited no detectable Cr content. However, following the reaction, the Cr content significantly increased to 0.9% (Figure 4f). This substantial rise clearly demonstrates that Cr was successfully adsorbed onto the surface of PEI@MMI(800).

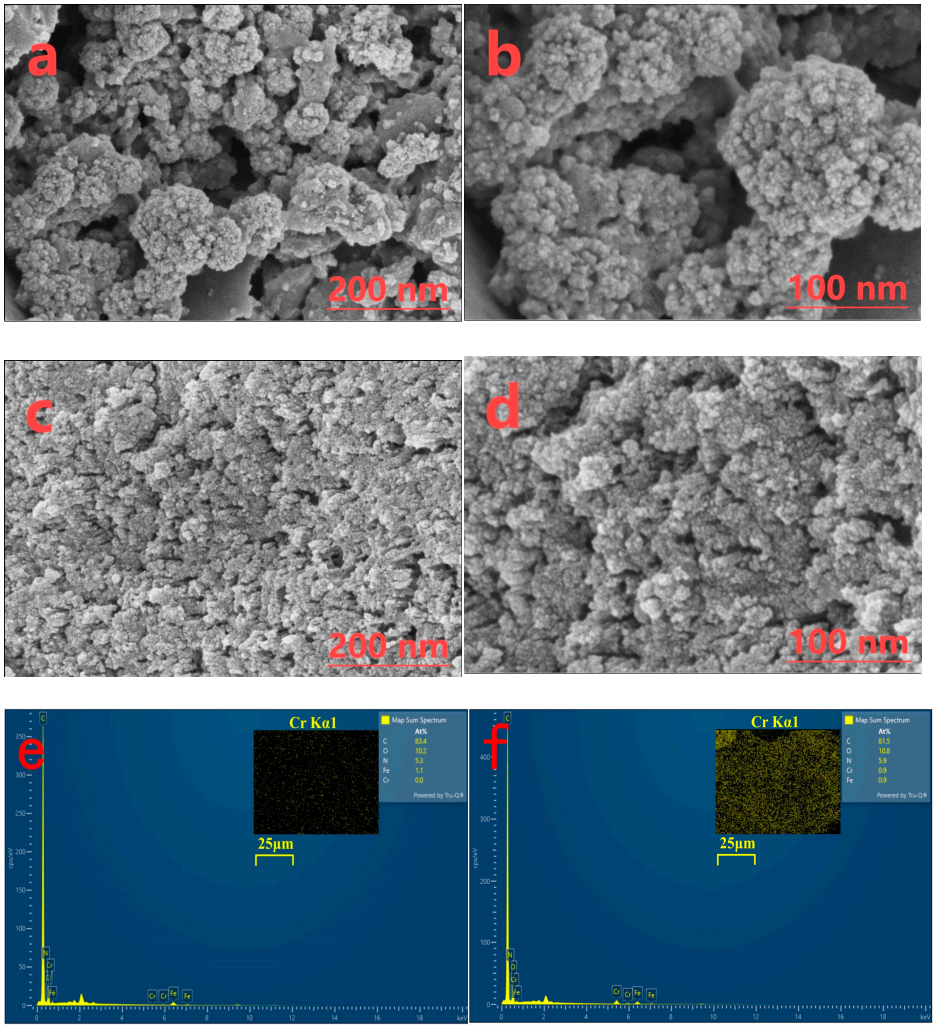

Figure 4. SEM morphologies of PEI@MMI(800) before Cr(VI) adsorption at magnifications of 50 k (**a**) and 100 k (**b**) and after Cr(VI) adsorption at magnifications of 50 k (**c**) and 100 k (**d**); SEM-EDS imaging of PEI@MMI(800) before (**e**) after Cr(VI) adsorption (**f**).

3.2.2. XRD

As shown in Figure 5, the diffraction peaks of MMI(800) at 30.05°, 35.47°, 53.29°, 56.98°, and 62.67° were attributed to Fe_3O_4, corresponding to the crystal plane reflections of (200), (016), (314), (232), and (228) in PDF#01-072-8152. The diffraction peaks at 41.86°, 60.69°, 72.66°, and 76.46° were attributed to FeO, corresponding to the crystal plane reflections of (200), (220), (311), and (222) in PDF#01-089-7100 [19]. The diffraction peaks at 44.67°, 65.02°, and 82.33° were attributed to Fe, corresponding to the crystal plane reflections of (110), (200), and (211) in PDF#00-006-0696 [20]. The diffraction peaks at 37.47°, 43.59°, 58.13°, 69.19°, and 70.54° were attributed to Fe_3C, corresponding to the crystal plane reflections of (121), (102), (231), (232), and (312) in PDF#04-007-0418 [21].

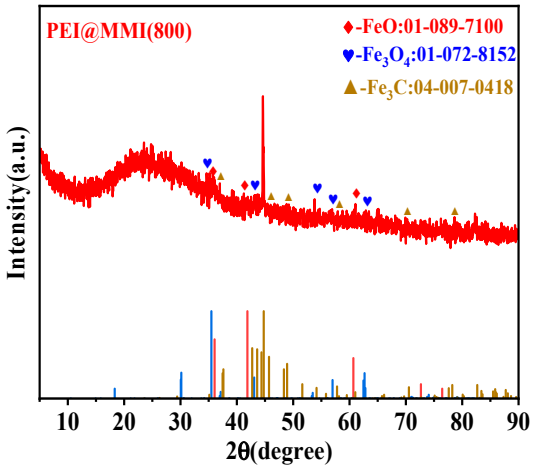

Figure 5. XRD pattern of PEI@MMI(800).

3.2.3. FTIR

The FTIR spectra of the sample before and after Cr(VI) adsorption are shown in Figure 6. A prominent peak at approximately 570 cm^{-1} is attributed to Fe-O vibrations in Fe_3O_4, originating from iron oxides in IBWS [22]. Peaks at 1067 cm^{-1}, 1541 cm^{-1}, and 1620 cm^{-1} are assigned to C-N stretching, N-H bending, and amine-related functionalities from the PEI coating, respectively [23–25]. After Cr(VI) adsorption, these peaks were still observed at comparable positions, with only minor changes (within ±4 cm^{-1}), which are considered to fall within the instrument's resolution limit and therefore are not interpreted as significant chemical shifts. Additionally, peaks around 2926 cm^{-1} and 3427 cm^{-1} correspond to CH_3 asymmetric stretching and O-H stretching vibrations, respectively [26,27]. After adsorption, slight variations in peak intensity were observed. However, these differences are more likely attributed to changes in the relative sample concentration and pellet preparation process, rather than direct interaction with Cr(VI). Thus, the FTIR results primarily confirm the presence of functional groups potentially involved in the adsorption process, while no definitive evidence of structural alteration can be inferred from peak shifting or intensity alone.

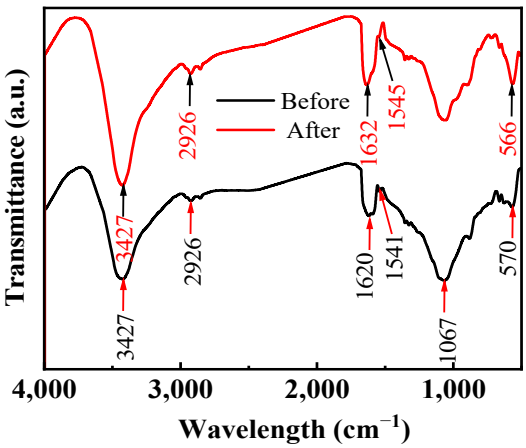

Figure 6. FTIR spectrum of PEI@MMI(800) before and after Cr(VI) adsorption.

3.3. Static Cr(VI) Adsorption

3.3.1. Effect of Solution pH

As shown in Figure 7a, the adsorption capacity of Cr(VI) decreased from 41.09 mg/g to 15.75 mg/g as the solution pH increased from 2 to 9, indicating that higher pH values had a negative impact on Cr(VI) adsorption. This trend can be explained by the surface charge

behavior of the adsorbent. As shown in Figure 7b, the zeta potential of PEI@MMI(800) decreased from +9.8 mV to −60.4 mV as the pH increased from 2 to 9, with the point of zero charge (pH_{ZPC}) occurring at approximately pH 3.21. In the pH range below 3.21, the PEI@MMI(800) adsorbent carried a positive charge and effectively adsorbed Cr(VI) ion, which exist mainly as oxyanion of $Cr_2O_7^{2-}$ in solution, through electrostatic attraction. This interaction led to higher Cr(VI) adsorption capacities. Conversely, at pH values above 3.21, the adsorbent surface became negatively charged and repelled the Cr(VI) oxyanions of $Cr_2O_7^{2-}$ and CrO_4^{2-} electrostatically, resulting in lower adsorption capacities.

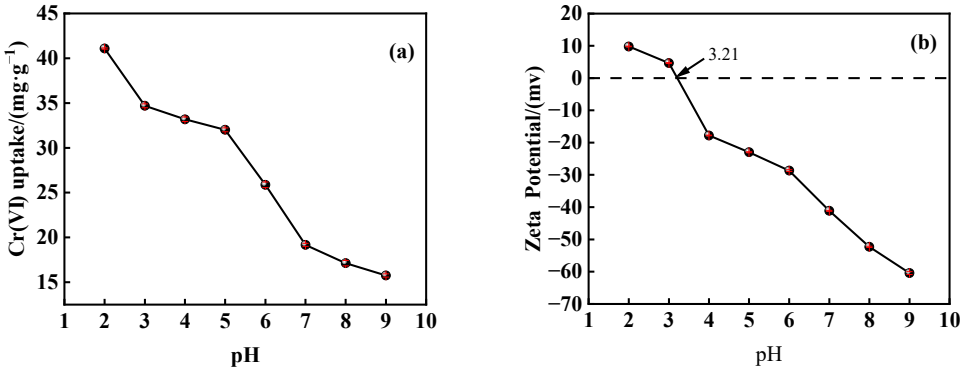

Figure 7. Influence of initial pH on Cr(VI) adsorption (**a**) and zeta potential (**b**) (C_0 = 100 mg/L, T = 25 °C).

Additionally, in the alkaline environment (pH > 7), the presence of hydroxide ions (OH^-) increased, which competed with Cr(VI) oxyanions for adsorption sites on the PEI@MMI(800) surface. This competition further weakened the adsorption of Cr(VI), contributing to the observed decline in adsorption capacity at higher pH values.

3.3.2. Adsorption Kinetics

Figure 8a depicts the nonlinear fitting of Cr(VI) adsorption by PEI@MMI(800) using three widely recognized kinetic models: the pseudo-first-order equation, the pseudo-second-order equation, and the intraparticle diffusion model (Equations (1)–(3)).

$$\ln(q_e - q_t) = \ln q_e - k_1 \cdot t \quad (1)$$

$$\frac{t}{q_t} = \frac{1}{k_2 \cdot q_e} + \frac{1}{q_e} \cdot t \quad (2)$$

$$q_t = k_b t^{0.5} + I \quad (3)$$

where q_e (mg/g) and q_t are the adsorption capacity at equilibrium and at time t, respectively; t (min) is the reaction time; k_1 (1/min) and k_2 (g/(mg·min)) are the pseudo-first-order and pseudo-second-order adsorption rate constants, respectively; k_b (mg/(g·$h^{0.5}$)) is the rate constant; and I (mg/g) is the intercept constant, respectively.

Table 1 presents the kinetic parameters obtained from model fitting. The pseudo-second-order model exhibited highere R^2 values than those of the first-second-order model, indicating a better fit to the experimental data. Additionally, the calculated equilibrium adsorption capacities (q_e) from the pseudo-second-order model were in close agreement with the experimentally obtained values: 19.820 mg/g for C_0 = 50 mg/L, 25.236 mg/g for C_0 = 75 mg/L, and 34.476 mg/g for C_0 = 100 mg/L. These results suggest that the pseudo-second-order model is more suitable for describing the kinetics of Cr(VI) adsorption by PEI@MMI(800).

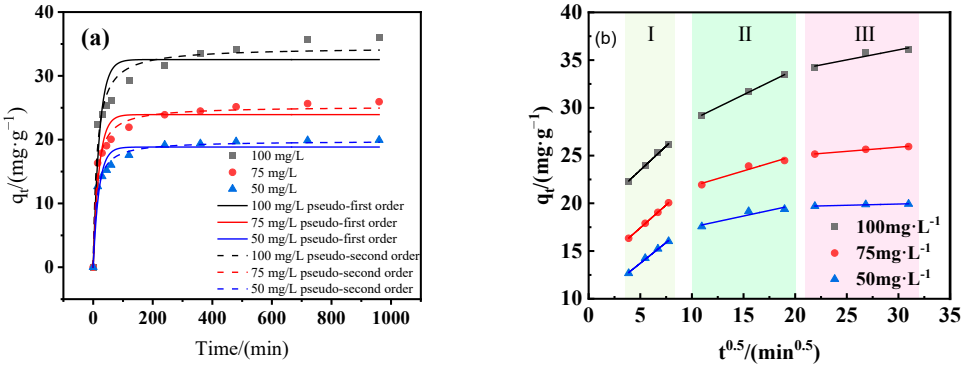

Figure 8. The nonlinear fitting results of the kinetic processes of Cr(VI) adsorption by PEI@MMI(800) (**a**) and the relationship between lnKL vs. 1/T (**b**) (pH = 5.1, T = 25 °C).

Table 1. The kinetic parameters of Cr(VI) adsorption by PEI@MMI(800).

Kinetic Models	Parameters	C_0 (mg/L)		
		50	75	100
Pseudo-first order	q_e (mg/g)	18.84	23.92	32.55
	k_1 (min^{-1})	0.0006	0.004	0.004
	R^2	0.945	0.928	0.902
Pseudo-second order	k_2 [g/(mg·min)]	0.00464	0.00350	0.00233
	q_e(mg/g)	19.820	25.236	34.476
	R^2	0.990	0.980	0.967
Intraparticle diffusion	k_{i1} [mg/(g·$min^{0.5}$)]	1.005	0.957	0.866
	C_1	18.445	12.641	9.392
	R_1^2	0.996	0.999	0.996
	k_{i2} [mg/(g·$min^{0.5}$)]	0.529	0.322	0.232
	C_2	22.318	18.561	15.187
	R_2^2	0.999	0.948	0.892
	k_{i3} [mg/(g·$min^{0.5}$)]	0.210	0.088	0.026
	C_3	29.765	23.253	19.139
	R_3^2	0.900	0.989	0.934

Consequently, the adsorption process is primarily dominated by chemisorption, which involves the formation of chemical bonds between the adsorbate (Cr(VI)) and the functional groups on the adsorbent surface (e.g., amine groups from PEI) [28]. This mechanism is consistent with the high R^2 values and the close match between the model-predicted and experimentally observed adsorption capacities.

The intraparticle diffusion model was employed to elucidate the diffusion processes and identify the rate-limiting steps involved in the adsorption of Cr(VI) by PEI@MMI(800). As shown in Figure 8b, each fitting curve exhibited multilinear characteristics, which correspond to distinct stages of the adsorption process: surface diffusion, intraparticle diffusion, and equilibrium adsorption [29]. The fact that none of the linear segments passed through the coordinate origin indicates that the adsorption of Cr(VI) by PEI@MMI(800) involved multiple adsorption mechanisms, rather than a single rate-limiting step [30].

Furthermore, for each initial Cr(VI) concentration, the intraparticle diffusion rate constants followed the order $k_{i1} > k_{i2} > k_{i3}$ (Table 1). This trend suggests that surface diffusion played a more dominant role in the initial stages of the adsorption process compared to the intraparticle diffusion [29]. This finding highlights the significance of surface interactions in facilitating rapid adsorption of Cr(VI) onto PEI@MMI(800), while intraparticle diffusion contributes to the subsequent stages of the process.

3.3.3. Adsorption Isotherm and Thermodynamics

Figure 9a shows that the equilibrium adsorption capacity (q_e) of Cr(VI) increased with the equilibrium Cr(VI) concentration (C_e) at all three temperatures. To further elucidate the mechanism underlying the Cr(VI) adsorption process by PEI@MMI(800), both the Langmuir and Freundlich models (Equations (4) and (5)) were employed to fit the experimental data.

$$\frac{C_e}{q_e} = \frac{1}{q_m \cdot k_L} + \frac{C_e}{q_m} \tag{4}$$

$$\ln q_e = \ln k_f + \frac{1}{n} \cdot \ln C_e \tag{5}$$

where q_m (mg/g) is the maximum Cr(VI) adsorption capacity; K_L (L/mg) is the constant of the Langmuir model, k_f (L·mg^{1-n}/g); and n is the constant of the Freundlich model.

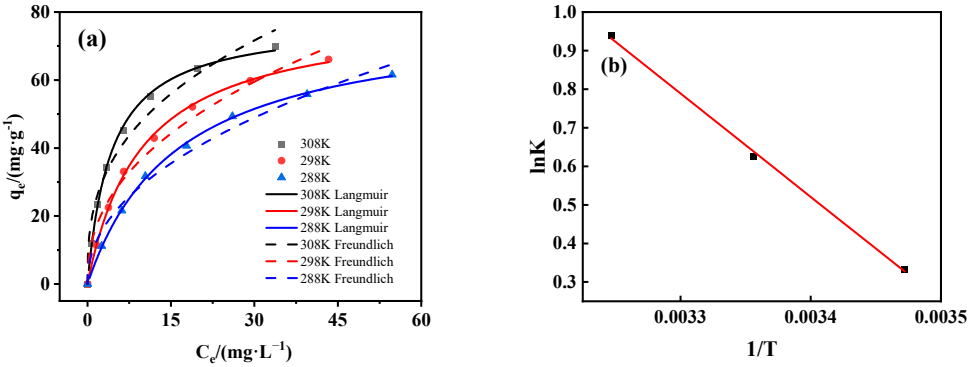

Figure 9. The nonlinear fitting using the Langmuir and Freundlich models (**a**) and the relationship between $\ln K_L$ vs. 1/T (**b**) (pH = 5.1, Time = 12 h).

As shown in Table 2, the Langmuir model exhibited higher R^2 values compared to the Freundlich model, indicating that the Langmuir model provided a better fit to the experimental data. This suggests that the adsorption of Cr(VI) by PEI@MMI(800) was more consistent with monolayer adsorption occurring on a homogeneous surface [3].

Table 2. The nonlinear fitting parameters of the Langmuir and Freundlich models.

T (K)	Langmuir			Freundlich		
	q_m (mg/g)	b	R^2	k_f (L^n·mg^{1-n}/g)	n	R^2
288	79.233	0.062	0.999	10.117	−0.463	0.981
298	79.927	0.103	0.998	13.897	−0.428	0.979
308	77.447	0.233	0.997	21.267	−0.357	0.969

To investigate the thermodynamics of Cr(VI) adsorption by PEI@MMI(800), ΔS^0, ΔG^0 and ΔH^0 were calculated using Equations (6)–(8).

$$\Delta G^0 = -RTlnK_L \tag{6}$$

$$\Delta G^0 = \Delta H^0 - T\Delta S^0 \tag{7}$$

$$lnK_L = \frac{-\Delta G^0}{RT} = \frac{\Delta S^0}{R} - \frac{\Delta H^0}{RT} \tag{8}$$

where K_L is the Langmuir constant; ΔG^0 (kJ/mol) is the free energy change; ΔH^0 (kJ/mol) is the standard enthalpy change; and ΔS^0 (kJ/mol·K) is the standard entropy change. ΔH^0

and ΔS^0 are derived from the Van't Hoff plots shown in Figure 9b. R and T represent the ideal gas constant (8.314 J/(mol·K)) and the reaction temperature (K), respectively.

Table 3 presents the results of the thermodynamic analysis. The negative values of ΔG^0 at all three reaction temperatures indicate that the adsorption of Cr(VI) by PEI@MMI(800) is a spontaneous process. The increasing absolute values of ΔG^0 with rising temperature further suggest that higher temperatures are more favorable for Cr(VI) adsorption [31]. Additionally, the positive ΔH^0 value indicates that the adsorption process is endothermic, meaning it absorbs heat from the surroundings. Meanwhile, the positive ΔS^0 value reveals an increase in disorder at the solid–liquid interface and enhanced stoichiometric interactions during the adsorption process [32].

Table 3. Thermodynamic parameters of Cr(VI) adsorption by PEI@MMI(800).

ΔS^0 (kJ/mol·K)	ΔH^0 (kJ/mol)	ΔG^0 (kJ/mol)		
		288	298	308
0.080	22.309	−0.731	−1.531	−2.331

3.3.4. Influence of Co-Existing Anions

Figure 10 depicts the influence of co-existing anions on the adsorption of Cr(VI) by PEI@MMI(800). The presence of Cl^-, SO_4^{2-}, and PO_4^{3-} weakened the adsorption of Cr(VI), with the adsorption capacity decreasing as the concentration of these anions increased. This observation can be attributed to the competition between Cr(VI), primarily existing as the oxyanion of $HCrO_4^-$ at pH 5.14, and the co-existing anions for the active adsorption sites on the surface of PEI@MMI(800) [33,34]. Specifically, the competitive effect of the anions on Cr(VI) adsorption followed the order $Cl^- < SO_4^{2-} < PO_4^{3-}$. This trend is likely due to the increasing negative charge of the anions, which enhances their competition with Cr(VI) for adsorption sites. Similar findings were reported when polyethylenimine-grafted nitrogen-doped magnetic biochar was used for aqueous Cr(VI) decontamination [35]. The higher the negative charge of the co-existing anions was, the stronger their competition with Cr(VI) for the active sites on the adsorbent surface. Consequently, the adsorption capacity of Cr(VI) by PEI@MMI decreased with increasing anion concentration.

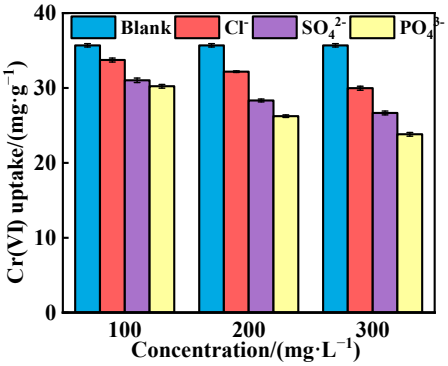

Figure 10. Influence of co-existing anions on adsorption by PEI@MMI (800) (pH = 5.1, C_0 = 100 mg/L, Time = 12 h).

3.3.5. Reusability of the Adsorbent

Figure 11 illustrates the reusability of PEI@MMI(800). The pristine PEI@MMI(800) exhibited a Cr(VI) adsorption capacity of 35.23 mg/g. After five cycles of regeneration, this capacity decreased to 28.11 mg/g, retaining 79.79% of its initial adsorption performance. This decline was attributed to the irreversibility of some adsorption sites on the surface of

PEI@MMI(800) following repeated use [31]. Additionally, the loss of active sites during the regeneration process further contributed to the reduced Cr(VI) adsorption capacity [31].

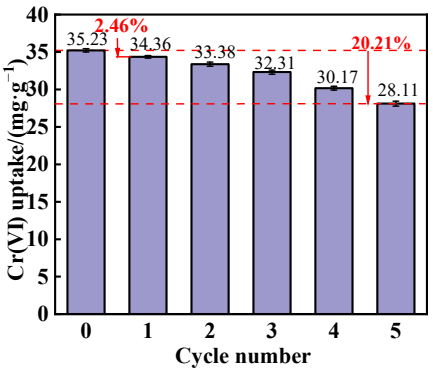

Figure 11. Recycling performance of PEI@MMI(800) across five cycles of Cr(VI) adsorption (pH = 5.1, C_0 = 100 mg/L, time = 12 h).

3.3.6. Cr(VI) Adsorption Mechanism Exploration

Upon comparison of the XPS full spectra before and after Cr(VI) adsorption, a pronounced Cr 2p binding energy peak emerged in the spectrum following the adsorption process (Figure 12a). This observation clearly demonstrated that Cr(VI) was effectively adsorbed onto the surface of PEI@MMI(800).

By examining the Fe 2p binding energy peaks before and after Cr(VI) adsorption (Figure 12b,c), it is evident that the shift in peak position for Fe 2p in PEI@MMI(800) was minimal. However, a notable change was observed in the area ratios of peaks associated with different valence states. Prior to adsorption, the Fe 2p peaks were primarily composed of the Fe 2p1/2 and Fe 2p3/2 spin–orbit doublets, along with satellite peaks. Specifically, the Fe 2p3/2 peak was mainly attributed to Fe^{2+} 2p3/2 (710.4 eV) and Fe^{3+} 2p3/2 (712.8 eV) [36].

The Fe 2p1/2 orbital is predominantly characterized by Fe^{2+} 2p1/2 (724.0 eV) and Fe^{3+} 2p1/2 (725.7 eV) [37]. Following the adsorption process, the proportion of Fe^{2+} binding energy in the Fe 2p peak decreased from 52.6% to 46.6%, while the proportion of Fe^{3+} binding energy increased from 33.9% to 38.4%. These changes, when compared to the values before Cr(VI) adsorption, suggest that Fe^{2+} participated in the reduction of Cr(VI) to Cr(III) and was subsequently oxidized to Fe^{3+} during the adsorption process (Equations (9) and (10)).

$$3Fe^{2+} + HCrO_4^- + 7H^+ \rightarrow 3Fe^{3+} + Cr^{3+} + 4H_2O \quad (9)$$

$$3Fe^{2+} + CrO_4^{2-} + 8H^+ \rightarrow 3Fe^{3+} + Cr^{3+} + 4H_2O \quad (10)$$

As illustrated in Figure 12d,e, the N1s binding energy spectra of PEI@MMI(800) before and after adsorption displayed two distinct binding energies. The characteristic peak at 399.3 eV was attributed to the N-H [38], and the peak at 401.5 eV belonged to the C-N [39], confirming the successful loading of PEI onto the surface of MMI. Following the adsorption of Cr(VI), the peak position of the N-H bond underwent a slight shift, and its relative peak area decreased from 77.6% to 67.5%. This observation indicated that the N-H participated in Cr(VI) removal by reducing it to Cr(III) (Equations (11) and (12)) [40].

$$7H^+ + HCrO_4^- + 3e^- + NH- \rightarrow -N = +Cr^{3+} + 4H_2O \quad (11)$$

$$7H^+ + CrO_4^{2-} + 2e^- + -NH- \rightarrow -N = +2Cr^{3+} + 4H_2O \quad (12)$$

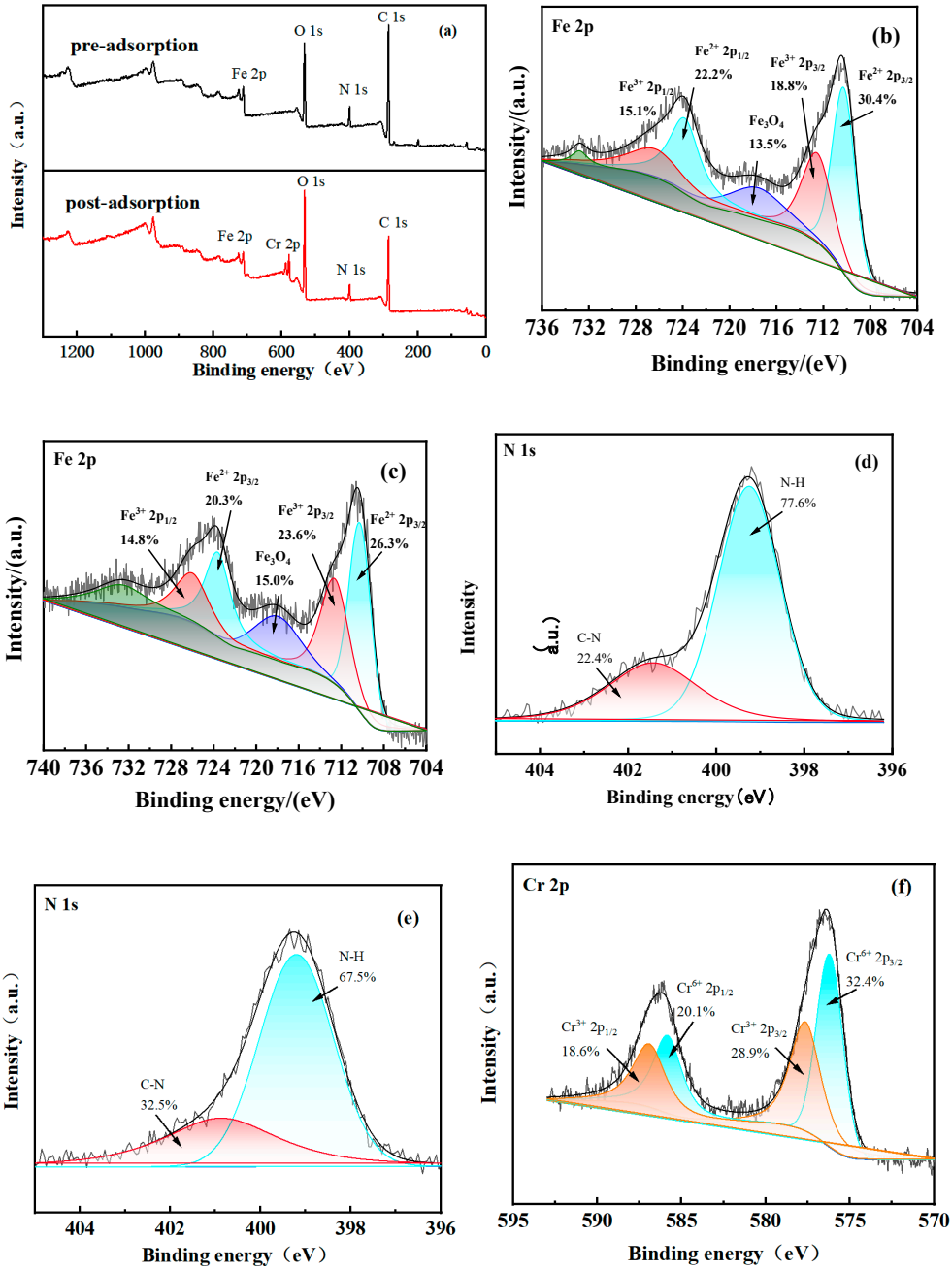

Figure 12. The full XPS spectrum of PEI@MMI(800) before and after Cr(VI) adsorption (**a**), the high-resolution spectrum of Fe 2P before and after Cr(VI) adsorption (**b**,**c**), the high-resolution spectrum of N 1s before and after Cr(VI) adsorption (**d**,**e**), and Cr 2P after Cr(VI) adsorption (**f**).

Meanwhile, the protonated amine and imine groups reacted with the negatively charged Cr (VI) species through electrostatic attraction and complexation in the acidic environment, thereby facilitating adsorption (Equations (13)–(15)) [41,42].

$$-NH_2 + H^+ \rightarrow NH_3^+ \quad (13)$$

$$NH_3^+ + HCrO_4^- \rightarrow -NH_3^+ \cdots HCrO_4^- \quad (14)$$

$$NH_3^+ + CrO_4^{2-} \rightarrow -NH_3^+ \cdots CrO_4^{2-} \quad (15)$$

As depicted in Figure 12f, the binding energies at 576.3 eV and 586.0 eV were assigned to Cr(VI) 2p3/2 and Cr(VI) 2p1/2, respectively, while the binding energies at 577.7 eV and

587.0 eV corresponded to Cr(III) 2p3/2 and Cr(III) 2p1/2, respectively [43]. It is evident that upon adsorption of Cr(VI) by PEI@MMI(800), the peak area attributed to Cr(III) increased from 0 to 47.5%. This significant change indicated that a considerable portion of Cr(VI) was reduced to Cr(III) during the adsorption process.

As previously stated, the process of Cr(VI) removal by PEI@MMI(800) is a multifaceted mechanism. It encompasses electrostatic adsorption, the chelation of Cr(VI) via PEI, and the reduction of Cr(VI) to Cr(III) (Figure 13).

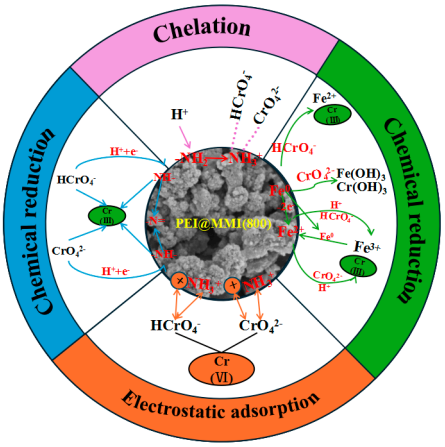

Figure 13. The mechanism of Cr(VI) removal by PEI@MMI(800).

4. Conclusions

In this study, activated carbon was employed to reduce iron-based waterwork sludge in a nitrogen environment at high temperature within a tube furnace, yielding magnetic multivalent iron. This material was further modified with polyethyleneimine (PEI) to synthesize the composite PEI@MMI(800). Static Cr(VI) adsorption tests were then conducted using PEI@MMI(800), leading to the following conclusions:

(1) The adsorption of Cr(VI) by PEI@MMI(800) was significantly influenced by pH. The Cr(VI) adsorption capacity decreased from 41.09 mg/g to 15.75 mg/g as the pH increased from 2 to 9, indicating a strong pH-dependent behavior.

(2) The adsorption process was well described by the pseudo-second-order kinetic model and the Langmuir isotherm model. Thermodynamic analysis revealed that the adsorption process was spontaneous and endothermic in nature.

(3) Cl^-, SO_4^{2-} and PO_4^{3-} weakened Cr(VI) adsorption, with their inhibitory effects following the order $Cl^- < SO_4^{2-} < PO_4^{3-}$. Additionally, higher concentrations of these anions led to lower Cr(VI) adsorption capacities.

(4) After five cycles of reuse, PEI@MMI(800) lost 20.21% of its initial Cr(VI) adsorption capacity, suggesting that while the composite exhibited good reusability, there was a gradual decline in performance over multiple cycles.

(5) The primary mechanisms for Cr(VI) removal by PEI@MMI(800) were identified as electrostatic adsorption, as well as chelation of Cr(VI) by PEI. Additionally, the reduction of Cr(VI) to Cr(III) significantly contributed to the overall removal efficiency.

These findings highlight the effectiveness and multifaceted nature of the PEI@MMI(800) composite in adsorbing and reducing Cr(VI) from aqueous solutions.

Author Contributions: Conceptualization, J.T. and Z.Y.; methodology, J.T., H.W. and Z.Y.; formal analysis, H.W., S.S. and J.Z.; writing—original draft preparation, J.Z., S.S. and X.D. writing—review and editing, J.T. and M.Y.; supervision, Z.Y.; funding acquisition, J.T. All authors have read and agreed to the published version of the manuscript.

Funding: This research is funded by the Henan Province Science and Technology Research and Development project (242102231015, 252102320359).

Data Availability Statement: The data presented in this study are available on request from the corresponding author due to privacy.

Conflicts of Interest: The authors declare no conflicts of interest.

References

1. Duan, J.; Chen, B.; Zhang, Y.; Cai, P.; Wang, F. Enhanced adsorption of Cr (VI) from aqueous solutions by CTAB-modified schwertmannite: Adsorption performance and mechanism. *Chem. Eng. Res. Des.* **2024**, *208*, 464–474. [CrossRef]
2. Göde, F.; Yılmaz, A.; Aktaş, A.H.; Pehlivan, E. Artificial neural network approach to model Cr (III) and Cr (VI) adsorption by NACS and BCS. *Appl. Water Sci.* **2024**, *14*, 28. [CrossRef]
3. Zahakifar, F.; Dashtinejad, M.; Sepehrian, H.; Samadfam, M.; Fasihi, J.; Yadollahi, A. Intensification of Cr (VI) adsorption using activated carbon adsorbent modified with ammonium persulfate. *Sci. Rep.* **2024**, *14*, 16949. [CrossRef]
4. Yang, F.; Jiang, Y.; Dai, M.; Hou, X.; Peng, C. Active biochar-supported iron oxides for Cr (VI) removal from groundwater: Kinetics, stability and the key role of FeO in electron-transfer mechanism. *J. Hazard. Mater.* **2022**, *424*, 127542. [CrossRef]
5. Karimi-Maleh, H.; Ayati, A.; Ghanbari, S.; Orooji, Y.; Tanhaei, B.; Karimi, F.; Alizadeh, M.; Rouhi, J.; Fu, L.; Sillanpää, M. Recent advances in removal techniques of Cr (VI) toxic ion from aqueous solution: A comprehensive review. *J. Mol. Liq.* **2021**, *329*, 115062. [CrossRef]
6. Geng, L.; Xu, W.; Chang, S.; Chen, S. Polyamidoamine dendrimers modified MXene and its high-performance adsorption behavior for Cr (VI). *J. Mol. Liq.* **2024**, *399*, 124406. [CrossRef]
7. Hu, W.; Zhang, X.; Chen, M.; Rahman, S.T.; Li, X.; Wang, G. Enhancing Cr (VI) Adsorption of Chestnut Shell Biochar through H_3PO_4 Activation and Nickel Doping. *Molecules* **2024**, *29*, 2220. [CrossRef]
8. Hou, B.; Yang, X.; Wang, L.; Shi, T.; Akram, M.; Wang, L.; Wan, J.; Gao, B.; Pan, J. Fe doping enhanced Cr (VI) adsorption efficiency of cerium-based adsorbents: Adsorption behaviors and inner removal mechanisms. *J. Colloid. Interface Sci.* **2024**, *673*, 216–227. [CrossRef]
9. Jia, Z.; Liang, F.; Wang, F.; Zhou, H.; Liang, P. Selective adsorption of Cr (VI) by nitrogen-doped hydrothermal carbon in binary system. *Environ. Geochem. Health* **2024**, *46*, 121. [CrossRef]
10. Jiang, S.; Yan, X.; Peacock, C.L.; Zhang, S.; Li, W.; Zhang, J.; Feng, X.; Liu, F.; Yin, H. Adsorption of Cr (VI) on Al-substituted hematites and its reduction and retention in the presence of Fe^{2+} under conditions similar to subsurface soil environments. *J. Hazard. Mater.* **2020**, *390*, 122014. [CrossRef]
11. Jiang, T.; Chai, J.; Wang, Y.; Du, Q.; Shi, J.; Xu, Z. Enhanced photocatalytic reduction of Cr (VI) from aqueous solution using Fe^0/TiO_2-based polymeric nanocomposites. *Environ. Sci. Pollut. Res.* **2023**, *30*, 110312–110323. [CrossRef] [PubMed]
12. Nelson, J.; Joe-Wong, C.; Maher, K. Cr (VI) reduction by Fe (II) sorbed to silica surfaces. *Chemosphere* **2019**, *234*, 98–107. [CrossRef] [PubMed]
13. Yang, Y.; Zhang, Y.; Wang, G.; Yang, Z.; Xian, J.; Yang, Y.; Li, T.; Pu, Y.; Jia, Y.; Li, Y.; et al. Adsorption and reduction of Cr (VI) by a novel nanoscale FeS/chitosan/biochar composite from aqueous solution. *J. Environ. Chem. Eng.* **2021**, *9*, 105407. [CrossRef]
14. Zhang, Q.; Ye, X.; Chen, D.; Xiao, W.; Zhao, S.; Li, J.; Li, H. Chromium(VI) removal from synthetic solution using novel zero-valent iron biochar composites derived from iron-rich sludge via one-pot synthesis. *J. Water Process Eng.* **2022**, *47*, 102720. [CrossRef]
15. Zheng, Z.; Duan, X.; Tie, J. One-pot synthesis of a magnetic Zn/iron-based sludge/biochar composite for aqueous Cr (VI) adsorption. *Environ. Technol. Innov.* **2022**, *28*, 102661. [CrossRef]
16. Yoo, S.-H.; Lee, S.-C.; Ko, M.; Yoon, S.; Lee, J.; Park, J.-A.; Kim, S.-B. Adsorption of Hg(II) on polyethyleneimine-functionalized carboxymethylcellulose beads: Characterization, toxicity tests, and adsorption experiments. *Int. J. Biol. Macromol.* **2023**, *241*, 124516. [CrossRef]
17. Zhang, Y.; Zhang, H.; Zhao, J.; Zhang, X.; Cao, Z.; Jiang, B. Efficient adsorption of fluoride ions by polyethyleneimine modified diatomite under different conditions in a fixed bed column. *Desalin. Water Treat.* **2023**, *307*, 153–161. [CrossRef]
18. Xu, D.; Zheng, S.; Sun, T.; Gao, G.; Sun, Y.; Jia, H.; Zhu, X. Simultaneous adsorption and reduction of Cr (VI) on Potamogeton·crispus biochar supported nanoscale zero-valent iron: Electro- and sepctro-chemical mechanism. *J. Taiwan Inst. Chem. Eng.* **2024**, *155*, 105259. [CrossRef]
19. Dai, M.; Liu, S.; Tan, X.; Chen, Q.; Ye, J.; Sun, A.; Liu, N. Peroxydisulfate activation by magnetic nanoflakes zero-valent iron/graphitized carbon composites for norfloxacin removal: Synergistic effect of $^1O_2$ with surface Fe(IV). *Sep. Purif. Technol.* **2024**, *342*, 126841. [CrossRef]

20. Song, Y.; Beyazay, T.; Tüysüz, H. Effect of Alkali-and Alkaline-Earth-Metal Promoters on Silica-Supported Co-Fe Alloy for Autocatalytic CO_2Fixation. *Angew. Chem. Int. Ed. Engl.* **2024**, *63*, e202316110. [CrossRef]
21. Gao, T.; Yu, S.; Chen, Y.; Li, X.; Tang, X.; Wu, S.; He, B.; Lan, H.; Li, S.; Yue, Q.; et al. Regulating the thickness of the carbon coating layer in iron/carbon heterostructures to enhance the catalytic performance for oxygen evolution reaction. *J. Colloid Interface Sci.* **2023**, *642*, 120–128. [CrossRef] [PubMed]
22. Alterary, S.S.; AlKhamees, A. Synthesis, surface modification, and characterization of Fe_3O_4@ SiO_2 core@ shell nanostructure. *Green Process. Synth.* **2021**, *10*, 384–391. [CrossRef]
23. Khoobi, M.; Khalilvand-Sedagheh, M.; Ramazani, A.; Asadgol, Z.; Forootanfar, H.; Faramarzi, M.A. Synthesis of polyethyleneimine (PEI) and β-cyclodextrin grafted PEI nanocomposites with magnetic cores for lipase immobilization and esterification. *J. Chem. Technol. Biotechnol.* **2016**, *91*, 375–384. [CrossRef]
24. Liu, C.-H.; Hsien, Y. Adsorption Behaviors of Nucleic Acid by Cationic Magnetic Nanoparticles. *Appl. Mech. Mater.* **2013**, *284–287*, 271–275. [CrossRef]
25. Mathumba, P.; Kuvarega, A.T.; Dlamini, L.N.; Malinga, S.P. Synthesis and characterisation of titanium dioxide nanoparticles prepared within hyperbranched polyethylenimine polymer template using a modified sol–gel method. *Mater. Lett.* **2017**, *195*, 172–177. [CrossRef]
26. Eid, M.E.-S. Polyethylenimine-functionalized magnetic amorphous carbon fabricated from oil palm leaves as a novel adsorbent for Hg(II) from aqueous solutions. *Egypt. J. Pet.* **2018**, *27*, 1051–1060. [CrossRef]
27. Hebbar, V.; Bhajantri, R. Conductivity study of thermally stabilized RuO_2/polythiophene nanocomposites. *AIP Conf. Proc.* **2018**, *1942*, 040007. [CrossRef]
28. Li, S.; Ye, S.; Zhang, W.; He, H.; Zhang, Y.; Xiong, M.; Chen, Y.; Wang, M.; Nie, Z. Magnetic Ion-Imprinted Materials for Selective Adsorption of Cr (VI): Adsorption Behavior and Mechanism Study. *Molecules* **2024**, *29*, 1952. [CrossRef]
29. Zheng, Z.; Zhao, B.; Guo, Y.; Guo, Y.; Pak, T.; Li, G. Preparation of mesoporous batatas biochar via soft-template method for high efficiency removal of tetracycline. *Sci. Total Environ.* **2021**, *787*, 147397. [CrossRef]
30. Lei, W.; Qi, M.; Song, J.; Li, H.; Wang, X.; Ma, Y.; Gao, Z. Adsorption of polyphenolic compounds by sodium alginate-modified starch nanoparticles in a multiphase system: Kinetic, thermodynamic and release characteristics studies. *Food Hydrocoll.* **2025**, *162*, 110900. [CrossRef]
31. Li, Z.; Wei, Y.; Wu, H.; Yuan, P.; Bu, H.; Tan, X. Efficient and sustainable phosphate removal and recovery from wastewater with zinc-substituted magnetite. *Sep. Purif. Technol.* **2025**, *360*, 130642. [CrossRef]
32. Sun, W.; Liu, C.; Liu, S.; Zhang, J.; Chen, H.; Qiu, Z. Effective adsorption of Congo red by an innovative biochar/LDH-derived MIL-100(Al): Investigation of coexisting pollutants and mechanism revelation. *Sep. Purif. Technol.* **2025**, *359*, 130670. [CrossRef]
33. Rong, K.; Li, X.; Yang, Q.; Liu, Z.; Yao, Q.; Zhang, Z.; Li, R.; Zhao, L. ZhengRemoval of aqueous Cr (VI) by green synthesized sulfide iron nanoparticles loaded corn straw biochar: Performance, mechanism, and DFT calculations. *Appl. Surf. Sci.* **2024**, *670*, 160729. [CrossRef]
34. Song, Y.; Gotoh, T.; Nakai, S. Hexavalent Chromium Removal by an Ascorbic Acid Functionalized Polymer Hydrogel Adsorbent: The Effect of Physicochemical Factors. *ACS Appl. Polym. Mater.* **2023**, *5*, 2105–2112. [CrossRef]
35. Qu, J.; Zhang, X.; Bi, F.; Wang, S.; Zhang, X.; Tao, Y.; Wang, Y.; Jiang, Z.; Zhang, Y. Polyethylenimine-grafted nitrogen-doping magnetic biochar for efficient Cr (VI) decontamination: Insights into synthesis and adsorption mechanisms. *Environ. Pollut.* **2022**, *313*, 120103. [CrossRef] [PubMed]
36. Ye, Y.; Wang, D.; Meng, H.; Du, M.; Lin, Y.; Dong, Z.; Wang, A.; Wang, Y. Flexible noble-metal-free Fe-based metallic glasses as highly efficient oxygen evolution electrodes. *J. Non-Cryst. Solids* **2024**, *646*, 123208. [CrossRef]
37. Lee, J.; Lee, H. Valence State and Catalytic Activity of Ni-Fe Oxide Embedded in Carbon Nanotube Catalysts. *Nanomaterials* **2024**, *14*, 2004. [CrossRef] [PubMed]
38. Liu, C.; Li, M.; Meng, J.; Hei, P.; Wang, J.; Song, Y.; Liu, X.-X. Electrochemical Storage of Ammonium Versus Metal Ions in Bimetallic Hydroxide for Sustainable Aqueous Batteries. *Adv. Funct. Mater.* **2023**, *34*, 2310437. [CrossRef]
39. Khalse, N.M.; De, M. Adsorptive desulfurization of thiophenic sulfur compounds using nitrogen modified graphene. *Sep. Purif. Technol.* **2024**, *331*, 125693. [CrossRef]
40. Liu, Z.; Shi, X.; Wei, B.; Liao, S. Preparation of MIL-53 (Cr) and MIL-101 (Cr)/reduced graphene oxide/polyaniline composites for Cr (VI) adsorption. *J. Porous Mater.* **2025**, *32*, 353–364. [CrossRef]
41. Huang, Y.; Wang, B.; Lv, J.; He, Y.; Zhang, H.; Li, W.; Li, Y.; Wågberg, T.; Hu, G. Facile synthesis of sodium lignosulfonate/polyethyleneimine/sodium alginate beads with ultra-high adsorption capacity for Cr (VI) removal from water. *J. Hazard. Mater.* **2022**, *436*, 129270. [CrossRef] [PubMed]

42. Mao, W.; Zhang, Y.; Luo, J.; Chen, L.; Guan, Y. Novel co-polymerization of polypyrrole/polyaniline on ferrate modified biochar composites for the efficient adsorption of hexavalent chromium in water. *Chemosphere* **2022**, *303*, 135254. [CrossRef] [PubMed]
43. Sun, W.; Wang, R.; Li, L.; Zhao, J.; Liu, B. Ultra-high capacity and anti-interference for Cr (VI) removal by tannin-polyvinylimine modified graphite carbon nitride. *J. Environ. Chem. Eng.* **2024**, *12*, 113131. [CrossRef]

Disclaimer/Publisher's Note: The statements, opinions and data contained in all publications are solely those of the individual author(s) and contributor(s) and not of MDPI and/or the editor(s). MDPI and/or the editor(s) disclaim responsibility for any injury to people or property resulting from any ideas, methods, instructions or products referred to in the content.